Fluid Dynamics Research 10 (1992) 229–250
North-Holland

FLUID DYNAMICS
RESEARCH

Improved predictability of two-dimensional turbulent flows using wavelet packet compression

Marie Farge [a], Eric Goirand [a], Yves Meyer [b], Frédéric Pascal [c] and Mladen Victor Wickerhauser [d]

[a] *LMD–CNRS, Ecole Normale Supérieure, Paris, France*
[b] *CEREMADE, Université Paris–Dauphine, Paris, France*
[c] *Laboratoire d'Analyse Numérique, Université Paris XI, Orsay, France*
[d] *Department of Mathematics, Washington University at St. Louis, St. Louis, MO 63130, USA*

Received 25 January 1992

Abstract. We propose to use new orthonormal wavelet packet bases, more efficient than the Fourier basis, to compress two-dimensional turbulent flows. We define the "best basis" of wavelet packets as the one which, for a given enstrophy density, condenses the L^2 norm into a minimum number of non-negligible wavelet packet coefficients. Coefficients below a threshold are discarded, reducing the number of degrees of freedom. We then compare the predictability of the original flow evolution with several such reductions, varying the number of retained coefficients, either from a Fourier basis, or from the best-basis of wavelet packets. We show that for a compression ratio of $1/2$, we still have a deterministic predictability using the wavelet packet best-basis, while it is lost when using the Fourier basis. Likewise, for compression ratios of $1/20$ and $1/200$ we still have statistical predictability using the wavelet packet best-basis, while it is lost when using the Fourier basis. In fact, the significant wavelet packet coefficients in the best-basis appear to correspond to coherent structures. The weak coefficients correspond to vorticity filaments, which are only passively advected by the coherent structures. In conclusion, the wavelet packet best-basis seems to distinguish the low-dimensional dynamically active part of the flow from the high-dimensional passive components. It gives us some hope of drastically reducing the number of degrees of freedom necessary to the computation of two-dimensional turbulent flows.

1. Introduction

Fully developed turbulence is commonly viewed from one of two alternative perspectives, one on either side of the Fourier transform. In physical space, we observe well localized coherent structures. We may wonder if there is universality in their shapes and elementary interactions. In Fourier space, we see transfers of energy and enstrophy between different wavenumbers. We may ask, for example, if the slope of the energy spectrum is universal, namely independent of the initial and boundary conditions, after sufficient time. Time already introduces a great simplification, since vastly different flows can have the same energy spectrum. If we now want to reconcile the physical with the Fourier space perspective, we have to define new orthonormal bases to decompose two-dimensional turbulent flows. We may define bases made up of *atoms*, which are smooth functions well localized in both physical *and* Fourier space. These basis elements are well localized in *phase space*, namely in

Correspondence to: M. Farge, LMD–CNRS, Ecole Normale Supérieure, 24 rue Lhomond, 75231 Paris cedex 05, France.

both space *and* wavenumber coordinates. A coherent structure, which is characterized by both a location and a shape, can be seen to be a superposition of those phase space atoms in what may be described as *molecules*.

Numerical experiments which produce dynamically stable turbulent flows result in vorticity fields which may be described as coherent structures separated by vorticity filaments. The coherent structures retain their shape for long periods of time and contain large amounts of enstrophy. The vorticity filaments, on the other hand, correspond to the weakest enstrophy regions. They are passively advected by the coherent structures and dissipated. We conjecture that such flows can be segmented into "strong" components corresponding to the coherent structures and "weak" components or filaments and that only the "strong" components need be retained to accurately approximate the flow.

How coherent structures form, which is still an open problem, may be approached as the condensation of atoms into molecules. The flow is segmented into such atoms; it may be analyzed at each instant, and the evolution of coherent structures may be followed by tracking these molecules. In fact, projection onto a limited number of molecules results in a reduction in the dimension of the problem. We can now test whether this reduction is meaningful relative to the dynamics of the flow.

To numerically integrate the time evolution of turbulent flows, we are presently using two kinds of orthonormal basis, either one that is well localized in space (finite differences, finite elements, or vortex methods), or one that is well localized in wavenumber (spectral methods). If the appropriate model for a turbulent flow is point vortices, then the first type of basis is better suited; if it is a superposition of waves, then the Fourier basis is preferable. In general, turbulent flows are not as simple as these two limit cases. We have to develop a mixed approach for the intermediate cases; therefore, we have to look for new bases. Phase space atoms provide a very flexible choice.

A particular library of phase space atoms is the *wavelet packets*, which include grid points, wavelets, and analogs of Fourier and windowed Fourier basis elements. Wavelet packets have the advantage of remarkable orthogonality properties. Very many combinations of wavelet packets yield orthonormal bases. We then select that orthonormal basis which best condenses the enstrophy onto a minimal number of nonnegligible coefficients. This minimal number happens to be a reasonable candidate for he *theoretical dimension* of the attractor, or the expected number of degrees of freedom among the coherent structures.

2. Decaying two-dimensional turbulent flow

The whole approach is "numerically experimental". It uses high-resolution direct numerical simulations of decaying two-dimensional turbulent flows, performed with a standard pseudospectral Galerkin method. We try to define more appropriate orthonormal bases, i.e., more economical in terms of degrees of freedom. This is one way to reduce the computational cost of integrating the flow evolution.

The Navier–Stokes equations describe the dynamics of a two-dimensional incompressible viscous flow. In the periodic plane $S = (0, 2\pi) \times (0, 2\pi) \in \mathbb{R}^2$ and in the absence of external forcing, these take the following form:

$$\begin{aligned} &\partial \boldsymbol{u}/\partial t + (\boldsymbol{u} \cdot \boldsymbol{\nabla})\boldsymbol{u} + \boldsymbol{\nabla} P - \nu \nabla^2 \boldsymbol{u} = \boldsymbol{0}, && \text{in } S \times \mathbb{R}^+, \\ &\boldsymbol{\nabla} \cdot \boldsymbol{u} = 0, && \text{in } S \times \mathbb{R}^+, \\ &\boldsymbol{u}(\boldsymbol{x}, 0) = \boldsymbol{u}_0(\boldsymbol{x}), && \text{in } S. \end{aligned} \tag{2.1}$$

We also impose periodic boundary conditions. Here $\boldsymbol{u}$ is the velocity field, P is the pressure field, and ν is the kinematic viscosity. We can rewrite these equations in terms of vorticity:

$$\omega = \partial u_2/\partial x_1 - \partial u_1/\partial x_2, \tag{2.2}$$

and streamfunction ψ defined such that:

$$\boldsymbol{u} = \begin{pmatrix} u_1 \\ u_2 \end{pmatrix} = \begin{pmatrix} -\partial\psi/\partial x_2 \\ \partial\psi/\partial x_1 \end{pmatrix}. \tag{2.3}$$

The Navier–Stokes equations then become:

$$\begin{aligned} &\partial\omega/\partial t + J(\psi, \omega) - \nu\nabla^2\omega = 0, && \text{in } \mathrm{S}\times\mathbb{R}^+, \\ &\omega = \nabla^2\psi, && \text{in } \mathrm{S}\times\mathbb{R}^+, \\ &\omega(\boldsymbol{x}, 0) = \omega_0(\boldsymbol{x}), && \text{in S}, \end{aligned} \tag{2.4}$$

again with periodic boundary conditions, and where the Jacobian operator is:

$$J(\psi, \omega) = \frac{\partial\psi}{\partial x_1}\frac{\partial\omega}{\partial x_2} - \frac{\partial\psi}{\partial x_2}\frac{\partial\omega}{\partial x_1}. \tag{2.5}$$

The initial vorticity field $\omega_0(\boldsymbol{x})$ is a fully developed turbulent flow, previously computed with some external forcing, which has reached a statistically steady state. The same integration is then performed without forcing. We can expand ω and ψ in their Fourier series over the periodic domain S:

$$\omega(\boldsymbol{x}, t) = \sum_{\boldsymbol{k}\in\mathbb{Z}^2} \hat{\omega}(\boldsymbol{k}, t)\, \exp(\mathrm{i}\boldsymbol{k}\cdot\boldsymbol{x}), \tag{2.6}$$

where

$$\hat{\omega}(\boldsymbol{k}, t) = \frac{1}{2\pi}\int_{\boldsymbol{x}\in\mathbb{R}^2} \omega(\boldsymbol{x}, t)\, \exp(-\mathrm{i}\boldsymbol{k}\cdot\boldsymbol{x})\, \mathrm{d}\boldsymbol{x},$$

and

$$\psi(\boldsymbol{x}, t) = \sum_{\boldsymbol{k}\in\mathbb{Z}^2} \hat{\psi}(\boldsymbol{k}, t)\, \exp(\mathrm{i}\boldsymbol{k}\cdot\boldsymbol{x}), \tag{2.7}$$

where

$$\hat{\psi}(\boldsymbol{k}, t) = \frac{1}{2\pi}\int_{\boldsymbol{x}\in\mathbb{R}^2} \psi(\boldsymbol{x}, t)\, \exp(-\mathrm{i}\boldsymbol{k}\cdot\boldsymbol{x})\, \mathrm{d}\boldsymbol{x}.$$

To integrate the Navier–Stokes equations we use a pseudospectral Galerkin method which consists in truncating the trigonometric expansion of the different variables to the first Fourier modes, lying in the range $0 \le |\boldsymbol{k}| < k_\mathrm{r}$, where k_r is the cutoff wavenumber which gives some fixed resolution. The time integration is done using an Adams–Bashforth scheme. The periodic plane S is sampled on 128^2 grid points in our simulation. For the subgrid scale model we use a hyperdissipation operator $-(-\nabla^2)^4$, which replaces the Laplacian operator in the Navier–Stokes equations.

We conjecture that coherent structures appearing in the vorticity field ω are superpositions of elements well localized in both position and wavenumber. We shall call the individual elements *atoms*, while their superpositions into coherent structures may be called *molecules*. It is possible to identify the atoms in a molecule: they are co-localized with it, and they are orthogonal to each other. The number of atoms in a molecule corresponds approximately to the number of degrees of freedom of the coherent structure.

3. Linear Fourier rank reduction

The "linear Fourier" rank reduction method consists of picking a wavenumber cutoff $k_c < k_r$, and setting to zero all components which lie outside that cutoff. This further band-limits the signal. The "rank-reduced" vorticity and streamfunction are thus

$$\omega^c(\boldsymbol{x}, t) = \sum_{\substack{\boldsymbol{k}\in\mathbb{Z}^2 \\ 0\le|\boldsymbol{k}|\le k_c}} \hat{\omega}(\boldsymbol{k}, t)\, \exp(\mathrm{i}\boldsymbol{k}\cdot\boldsymbol{x}), \tag{3.1}$$

$$\psi^c(\boldsymbol{x}, t) = \sum_{\substack{\boldsymbol{k}\in\mathbb{Z}^2 \\ 0\le|\boldsymbol{k}|\le k_c}} \hat{\psi}(\boldsymbol{k}, t)\, \exp(\mathrm{i}\boldsymbol{k}\cdot\boldsymbol{x}). \tag{3.2}$$

The value of k_c is chosen such that the total number of lattice points inside a circle of radius k_c is the desired fraction of the original rank of the problem.

Truncation to the lowest wavenumbers is the traditional method of reducing the number of degrees of freedom in a computational turbulence problem. This method makes the assumption that the two-dimensional spectrum is vanishingly small at the cutoff wavenumbers, which is not true in general. If we truncate at a wavenumber where the spectrum contains significant energy, the method introduces artifacts. A "nonlinear" alternative to this truncation would be to first sort all Fourier components in decreasing order of absolute value, and then retain only the first few or largest modes. This method chooses coefficients independently of wavenumber. It cuts out only that part of the two-dimensional spectrum which contains very little energy, and therefore introduces far less significant artifacts. While this nonlinear approach to Fourier rank reduction looks promising, it is not well suited to the present pseudospectral integration methods. Their computational cost is dominated by the fast Fourier transform, which itself is controlled by the spectral bandwidth. In general, the spectral bandwidth of the nonlinear Fourier rank reduction is the same as that of the original.

4. Wavelet packets

Suppose f is a square-integrable function with $\| f \| \overset{\text{def}}{=} (\int_{\mathbb{R}} | f(x) |^2 \, \mathrm{d}x)^{1/2} = 1$. Let $\mathscr{B}$ be any collection of complete orthonormal bases for such functions. We may call $\mathscr{B}$ a *library of bases*. Now define the *dimension of f in basis B* as:

$$d_B = \exp\Big(- \sum_{b\in B} |\langle f, b\rangle|^2 \log |\langle f, b\rangle|^2 \Big),$$

where each b is one vector in the orthonormal basis B. Roughly speaking, this expression measures how many non-negligible coefficients are present in the expansion of f in basis B. The *theoretical dimension of f in the library* $\mathscr{B}$ is the minimum value of d_B, taken over all the orthonormal bases in the library $\mathscr{B}$. In the context of turbulent flow dynamics, the theoretical dimension may be related to the dimension of the inertial manifold [10,5].

Wavelet packets are generalizations of the compactly supported wavelets introduced by Daubechies [4], Mallat [6], and Meyer [7]. They constitute an overabundant set of basis functions with remarkable orthogonality properties, such that very many subsets form orthonormal bases; thus they form a library in the above sense. The one-dimensional case is described in refs. [2,3]. Each basis element is characterized by three attributes: position p, scale s, and wavenumber k. We shall shortly describe one of these elements $\psi_{p,s,k}$, which will be a square-integrable function of prescribed smoothness, located in the vicinity of $x = p$, and with approximately k oscillations or zero-crossings. Such a function is well localized in both

position and wavenumber, at the point (p, k) of *phase space*. By the Heisenberg uncertainty principle, it is not possible to localize a function to arbitrary precision in both p and k; we must have $\delta p \cdot \delta k \geq 1$ in normalized units, where δp is the uncertainty in position and δk is the uncertainty in wavenumber. In our construction, we have $\delta p \approx 2^s$ and $\delta k \approx 2^{-s}$ in the same normalization, so that the product of the uncertainties is roughly as small as possible. Such functions $\psi_{p,s,k}$, which cannot be significantly better localized in phase space, are what we shall call *atoms*.

Fourier analysis with such waveforms or atoms consists of calculating the "wavelet packet transform" $w_{p,s,k}(f) = \langle f, \psi_{p,s,k} \rangle$. Certain subsets of the indices (p, s, k) give orthonormal bases B and for these subsets we have the inversion formula:

$$f = \sum_{(p,s,k)\in \mathrm{B}} \langle f, \psi_{p,s,k} \rangle \psi_{p,s,k}. \tag{4.1}$$

Wavelet packets are rarely constructed explicitly. More usually, we simply apply the following fast discrete algorithm (described in refs. [2,3]) to the sampled values of f, and thereby produce the coefficients $w_{p,s,k}(f)$.

We introduce two (short) finite sequences $\{h_n\}$ and $\{g_n\}$, called "quadrature mirror filters", which satisfy the relations:

$$\begin{aligned}
&\sum_n h_{2n} = \sum_n h_{2n+1} = \tfrac{1}{2}\sqrt{2}\,, \quad g_n = (-1)^n h_{1-n}, \quad \forall n, \\
&\sum_n h_n h_{n+2m} = \sum_n g_n g_{n+2m} = \begin{cases} 1 & \text{if } m = 0, \\ 0 & \text{otherwise,} \end{cases} \\
&\sum_n h_n g_{n+2m} = 0, \quad \forall m \in \mathbb{Z}.
\end{aligned} \tag{4.2}$$

Consider for simplicity the one-dimensional case. Let $\phi = \phi(x)$ be any solution to the fixed-point equation

$$\phi(x) = \sqrt{2} \sum_j h_j \phi(2x + j).$$

Starting with a signal f, we compute $w_{p,s,k}(f)$ recursively from a resolution L as follows:

$$\begin{aligned}
w_{n,0,0}(f) &= \int_{\mathbb{R}} f(x) \phi(2^L x - n)\, \mathrm{d}x, \\
w_{n,s+1,2k}(f) &= \sum_j h_{2n+j} w_{j,s,k}(f), \\
w_{n,s+1,2k+1}(f) &= \sum_j g_{2n+j} w_{j,s,k}(f).
\end{aligned}$$

Observe that this defines all the coefficients $w_{p,s,k}(f)$ for $s \geq 0$, $p \in \mathbb{Z}$, and $0 \leq k < 2^s$. The index k is a frequency parameter, and is limited in its range by the Nyquist theorem: we cannot detect more than $N/2$ frequencies in an N-point time series. For the experiments in this article, we used the so-called "C6" coefficients, with h_n given below:

$$\begin{aligned}
&h_0 = 0.038580777747886749, \quad h_1 = -0.126969125396205200, \\
&h_2 = -0.077161555495773498, \quad h_3 = -0.607491641385684120, \\
&h_4 = 0.745687558934434280, \quad h_5 = 0.226584265197068560,
\end{aligned} \tag{4.3}$$

and $h_n = 0$ for all values of n outside [0, 5]; then we determine g_n from (4.2).

We claim now (and it is shown in refs. [2,3,11] that there are underlying functions $\psi_{p,k,s}$ and that the recursive computation of $w_{p,s,k}(f)$ is equivalent to calculating inner products of f

with these functions. We also avoid the initial inner product with ϕ by using the approximation $w_{n,0,0} \approx f(n2^{-L})$, which for smooth f and ϕ converges rapidly to the correct value as $L \to \infty$.

The underlying functions ψ are built up in two steps. We first define a family of functions recursively for integers $k \geq 0$ by

$$W_{2k}(x) = \sqrt{2} \sum_n h_n W_k(2x - n), \tag{4.4}$$

$$W_{2k+1}(x) = \sqrt{2} \sum_n g_n W_k(2x - n). \tag{4.5}$$

Note that W_0 satisfies the same fixed-point equation as ϕ. If we impose $\int \phi = 1$, then conditions (4.2) ensure that a unique solution to this fixed-point problem exists, and the quadrature mirror filters can be chosen (see ref. [4]) so that the solution has a prescribed degree of smoothness. Equations (4.2), (4.4), and (4.5) all have periodic analogs, which we use in the case of periodic boundary conditions.

One-dimensional wavelet packets are defined from these W_k by the formula

$$\psi_{p,s,k} = 2^{s/2} W_k(2^s - p). \tag{4.6}$$

Our library of basis functions in two dimensions consisted of the tensor products of the ψ functions. Let I be a dyadic square $2^{-s}[k_x, k_x + 1] \times 2^{-s}[k_y, k_y + 1]$ and put $\psi_{\mathrm{I},(p_x,p_y)}(x, y) = 2^s W_{k_x}(2^s x - p_x) W_{k_y}(2^s y - p_y)$. Then every basis in our library, for functions on the $2^S \times 2^S$ grid, corresponds to a set of the form:

$$\left\{ \psi_{\mathrm{I},(p_x,p_y)} : \mathrm{I} \in \mathcal{S},\ p_x \in \mathbb{Z},\ p_y \in \mathbb{Z},\ 0 \leq p_x < 2^{S-s},\ 0 \leq p_y < 2^{S-s} \right\}, \tag{4.7}$$

where $\mathcal{S}$ is a disjoint cover of the unit square by such dyadic squares I, for $s \geq 0$ and $0 \leq k_x, k_y < 2^{s-1}$. Computation of inner products with all ψ_{I} is performed recursively, as is the search for the best-basis; this two-dimensional version of the algorithm in refs. [2,3] is detailed in ref. [11]. The entire procedure has complexity $O(N \log N)$ where N is the rank of the problem, and $N = 2^{2S}$ for the original grid-point formulation.

The "best-basis of wavelet packets" rank reduction method consists of minimizing the theoretical dimension d of our initial vorticity field over such bases. Call the optimal basis B_*. We then project onto the top few coefficients as below:

$$\omega^{\mathrm{c}} = \sum_{\substack{\mathrm{I} \in \mathrm{B}_* \\ |c_{\mathrm{I}}| > \epsilon}} c_{\mathrm{I}} \psi_{\mathrm{I}},$$

where $c_{\mathrm{I}} = \langle \omega, \psi_{\mathrm{I}} \rangle$ and ϵ is some predetermined threshold, and we also sum over all integer translates (p_x, p_y), even though that notation is suppressed for compactness.

After projection onto the largest wavelet packet coefficients, what remains is expected to contain the remaining degrees of freedom of the entire system, whose theoretical dimension should be much greater than that of retained coefficients, which themselves should have the theoretical dimension of the approximate inertial manifold.

5. Numerical experiments

In all experiments we begin with an initial condition consisting of a fully developed two-dimensional turbulent flow samples on 128^2 grid points. This gives us a "reference initial flow field" (fig. 1a). We then integrate the evolution equation for an additional 6000 time steps between $t = 0.0$ and $t = 0.6$, using the numerical model defined in the previous section.

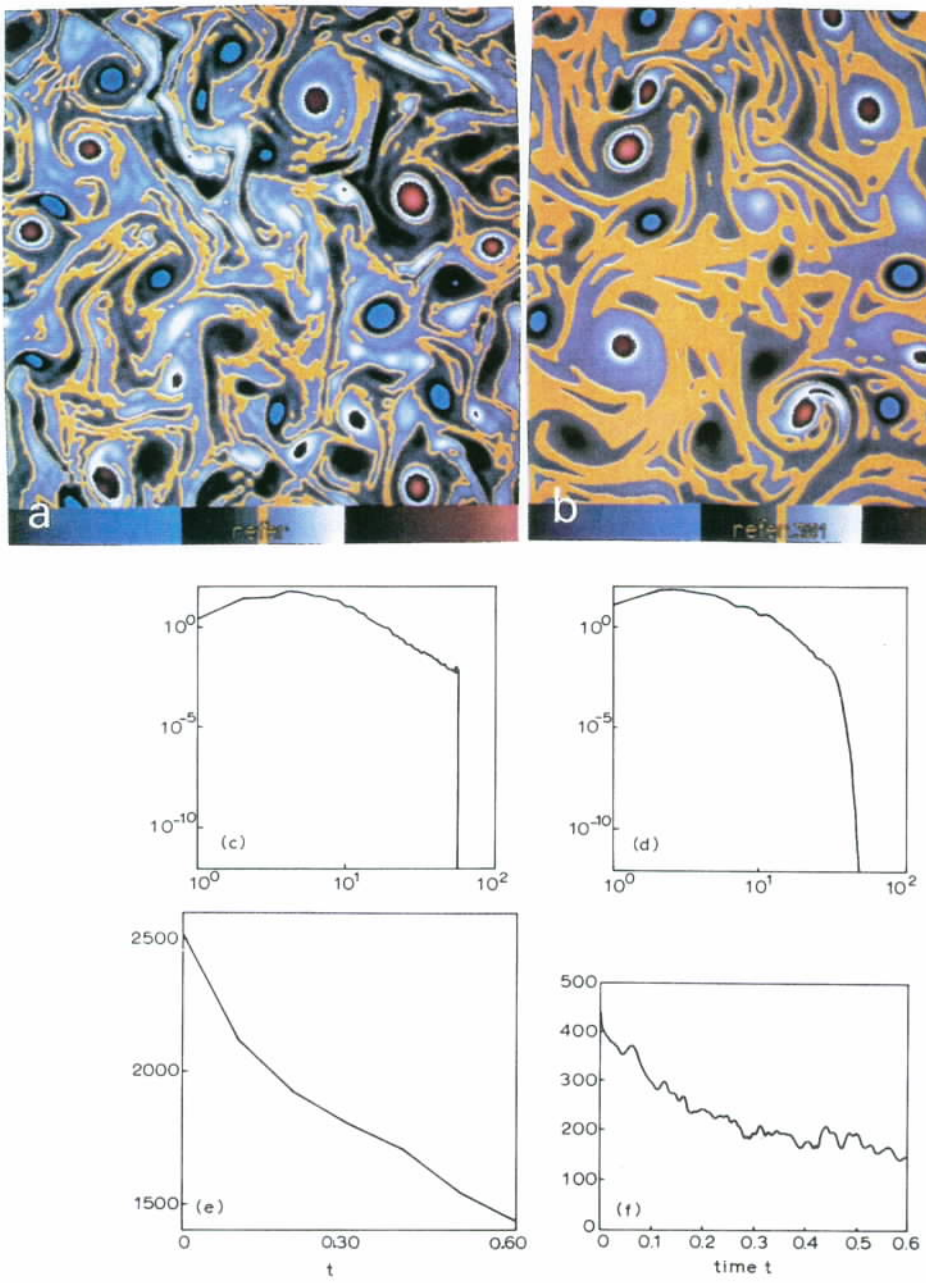

Fig. 1. Reference solution. (a) Vorticity field at $t = 0$, (b) vorticity field at $t = 0.6$, (c) energy spectrum at $t = 0$, (d) energy spectrum at $t = 0.6$, (e) evolution of enstrophy, (f) evolution of theoretical dimension. In all the following colour plates, the same colour scale, depicted in (a) and (b) is used.

In our normalization, this interval is approximately 30 eddy turnover times, or the time it takes for an average vortex to make 30 rotations. The resulting evolution will be called the "reference flow field evolution". In fig. 1 may be seen the vorticity fields at $t = 0.0$ (fig. 1a) and $t = 0.6$ (fig. 1b), as well as the power spectra of the initial (fig. 1c) and final (fig. 1d) vorticity fields, and the evolution of enstrophy (fig. 1e) and theoretical dimension (fig. 1f).

We then repeat the simulation using "rank-reduced initial flow fields", which are low-rank projections of the reference initial flow field. Rank reduction is obtained by expanding the initial state over an orthonormal basis, and then keeping only a fraction of the coefficients, the "strong" components. This was done in two ways:

(1) "Linear Fourier", which retains that fraction of the Fourier components at lowest strongest wavenumbers between $k = 0$ and a given cutoff $k = k_c$. This is a linear projection onto a lower-rank subspace.

(2) "Best-basis of wavelet packets", which retains a fixed fraction of the strongest coefficients in the wavelet packets basis chosen by the best-basis algorithm. Both the best basis algorithm and the subsequent choice of coefficients depends in a nonlinear way on the field.

After rank reduction, we reconstruct the original 128^2 grid point parameters. We then compute the evolution from the rank-reduced initial flow field to obtain the "rank-reduced flow field evolution". Both of these computations are performed using the same pseudospectral code as the reference, for the same duration of 6000 time steps. We also evolve the initial flow field consisting of the "weak" components discarded by rank reduction.

We expect the retained or "strong" components to be a good approximation to the reference flow, but we are concerned that some vital dynamical features might be discarded with the "weak" components. Our rank reduction goes too far if the discarded components contain coherent structures, or features which evolve on short time scales. The "weak" components affect the original flow in rough proportion to the fraction of the total enstrophy they contain, but the real extent of their contribution depends upon whether they resemble homogeneous noise or weakened coherent structures. The less the discarded components behave like the reference flow, the more confidence we have in the faithfulness of the approximation by the "strong" components.

For each method we consider three compression ratios: 2, 20, and 200. Here, the compression ratio is defined to be the reciprocal of the fraction of coefficients retained, which are 50%, 5% and 0.5%. We compute the evolution of both the "strong" components (those retained), and the "weak" components (those discarded or filtered out). We present initial and final vorticity fields for the two sets of components, and we also plot their initial and final energy spectra. Finally, we compute the evolution of enstrophy and theoretical dimension from both the weak and strong rank-reduced initial flow fields, to get weak and strong rank-reduced flow field evolutions. For the theoretical dimension evolution, we compute a value only every 20th time step, for a total of 300 values.

The evolution of the flow field does not conserve energy, but energy is a useful measure of the division introduced by the rank-reduction. We tabulate the initial and final energy of the 13 evolutions in table 1. The decomposition of the initial flow field into "strong" and "weak" wavelet packet components conserves enstrophy but not necessarily energy. In fact, the deviation from energy conservation indicates whether dynamically important components have been discarded. This is very noticeable in the 0.5–99.5% decomposition into wavelet packets. However, the linear decomposition of the initial flow field into Fourier modes does conserve energy at that time slice, though the evolutions thenceforth separate so the sum of the energies of the evolving pieces departs from the energy in the reference.

5.1. Linear Fourier rank reduction

5.1.1. "Strong" coefficients

We describe first the results for linear Fourier rank reduction. When 50% of the coefficients are retained (compression ratio 2), the resulting rank-reduced initial vorticity field is virtually identical to the reference (compare fig. 1a and fig. 2b). Likewise, the energy

Table 1
Initial and final energy of the flow-field evolutions.

Flow field	Energy (initial → final)
reference	49.53 → 48.48
50% strongest wavelet packets	49.52 → 48.46
5% strongest wavelet packets	47.12 → 46.37
0.5% strongest wavelet packets	43.97 → 43.72
50% lowest-wavenumber Fourier modes	49.47 → 48.52
5% lowest-wavenumber Fourier modes	44.64 → 43.99
0.5% lowest-wavenumber Fourier modes	6.06 → 6.06
50% weakest wavelet packets	0.0009 → 0.0005
95% weakest wavelet packets	1.72 → 1.52
99.5% weakest wavelet packets	24.70 → 23.95
50% highest-wavenumber Fourier modes	0.06 → 0.00
95% highest-wavenumber Fourier modes	4.90 → 4.16
99.5% highest-wavenumber Fourier modes	43.47 → 42.55

spectra are nearly identical (compare fig. 1c and fig. 4b). The evolution is statistically similar to the reference, but deterministically slightly different (compare the final fields in fig. 1b and fig. 6b, and the final spectra in fig. 1c and fig. 8b). Notice that in the center bottom of fig. 6b, there are two distinct red vortices which in the reference flow (fig. 1b) have merged, forever separating the two histories. The other differences, which are minor in terms of dynamics, are caused by the phase shift due to the enstrophy lost during rank reduction. The enstrophy and theoretical dimension both decrease slowly and very much like the reference (compare fig. 1e and fig. 10b and also 1f and 12b).

When 5% of the Fourier coefficients are retained (compression ratio 20), there is some noticeable distortion in both the vorticity field and the energy spectrum (compare fig. 1a and fig. 2d, and fig. 1c and fig. 4d). The evolution is deterministically quite different, and also statistically different (compare the final fields in fig. 1b and fig. 6d, and the final spectra in fig. 1d and fig. 8d). What is more, the enstrophy changes in a rather different manner (compare fig. 1e and fig. 10d). Finally, the theoretical dimension is greatly reduced by the rank reduction, and only after time $t = 0.1$ or so does it recover the dimension of the reference (compare fig. 1f and fig. 12d).

These distortions are even more pronounced when only 0.5% of the Fourier coefficients are retained (compression ratio 200). The rank-reduced initial field bears little resemblance to the reference (compare fig. 1a with fig. 2f). Only those components with the very lowest wavenumbers survive such drastic filtering, and the resulting field is much smoother than the reference. Of course the truncation in wavenumber has the expected effect on the energy spectrum (compare fig. 1c and fig. 4f). There are significant differences between the final vorticity fields and energy spectra of the reference and the rank-reduced evolution; the results bear little deterministic or statistical resemblance to the reference solution (compare the final field in fig. 1b with fig. 6f, and the final spectra in fig. 1d and fig. 8f). In particular the spectral slope in the inertial region is very different. The enstrophy of the rank-reduced field evolves quite differently from that of the reference (compare fig. 1e to fig. 10f), starting at a much lower level but decreasing much less, indicating that most of the dissipation occurs among the neglected terms. The theoretical dimension evolved very differently, even increasing while that of the reference is decreasing (compare fig. 1f to fig. 12f). Clearly the discarded terms contain dynamically important flow components.

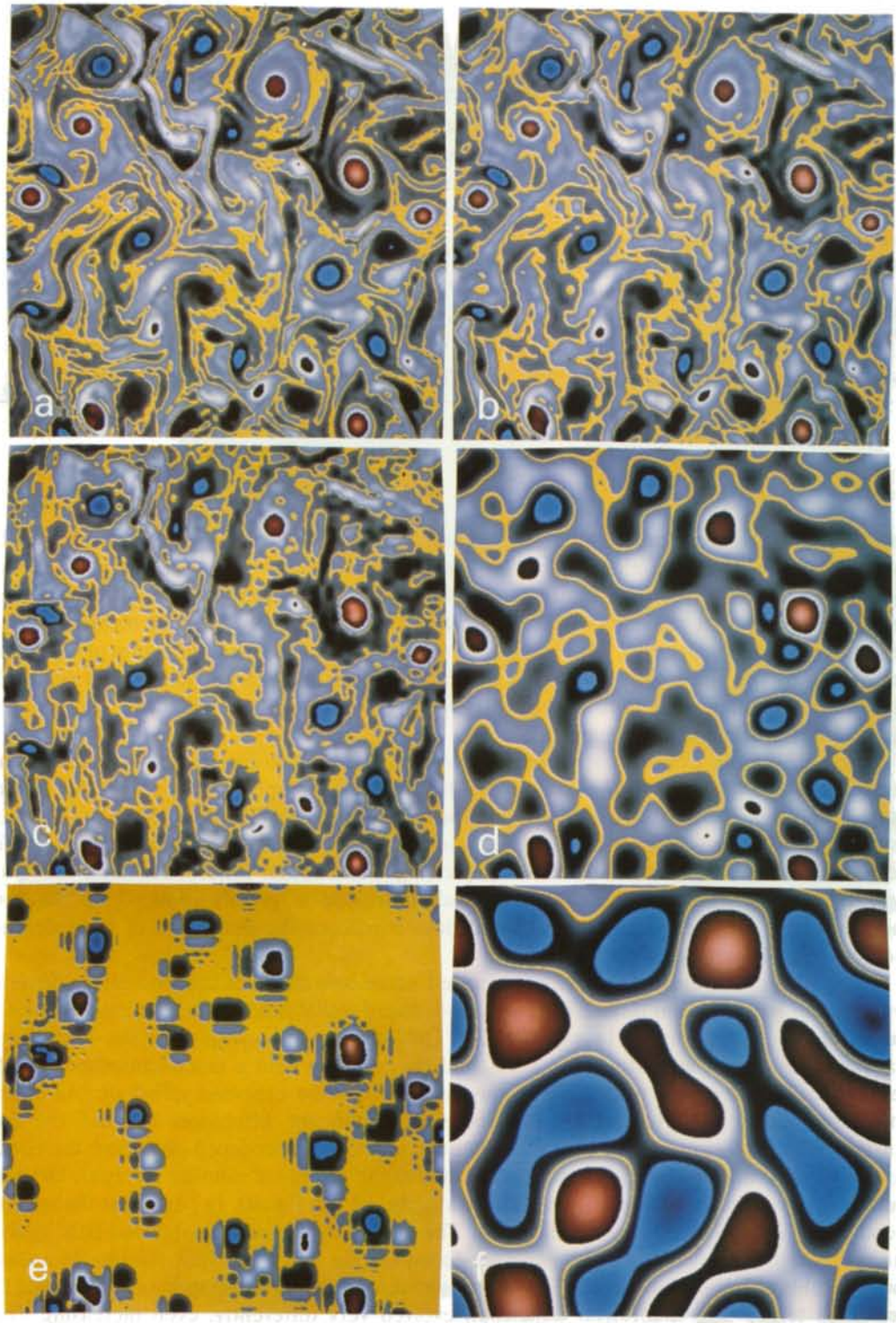

Fig. 2. Vorticity fields: "strong" components at $t = 0$. (a) Wavelet packet: 50% strongest, (b) linear Fourier: lowest-wavenumber 50%, (c) wavelet packet: 5% strongest, (d) linear Fourier: lowest-wavenumber 5%, (e) wavelet packet: 0.5% strongest, (f) linear Fourier: lowest-wavenumber 0.5%.

Fig. 3. Vorticity fields: "weak" components at $t = 0$. (a) Wavelet packet: 50% weakest, (b) linear Fourier: highest-wavenumber 50%, (c) wavelet packet: 95% weakest, (d) linear Fourier: highest-wavenumber 95%, (e) wavelet packet: 99.5% weakest, (f) linear Fourier: highest-wavenumber 99.5%.

5.1.2. "Weak" coefficients

Second, we repeated the simulation, but this time retaining only the terms which were rejected previously. For linear Fourier, this means those components with wavenumber above the cutoff $k = k_c$. Whether we started with the outer 50%, 95%, or 99.5% of the "weak" Fourier components, the rank-reduced initial vorticity field contains some nonnegligible enstrophy (see figs. 11b, d, f). That these fields (figs. 3b, d, f) contribute to the flow dynamics is seen in the final frames (figs. 7b, d, f), which have all evolved away from the initial fields. Even at 50% rank reduction, there is a fast time-scale evolution between $t = 0.2$ and $t = 0.3$ (see fig. 13b). Likewise, the energy spectra of the 95% and 99.5% "weak" components bear quite a bit of resemblance to the spectra of the reference, particularly at the end of the evolution (compare fig. 1d with figs. 9d, f). The spectrum of the 50% "weak" components, however, looks very much like white noise (see fig. 9b). The enstrophy of the 50% weak components decays to zero by $t = 0.1$ (see fig. 11b), but for the two other cases (see figs. 11d, f) the enstrophy evolves quite similarly to that of the reference (fig. 1e), indicating the

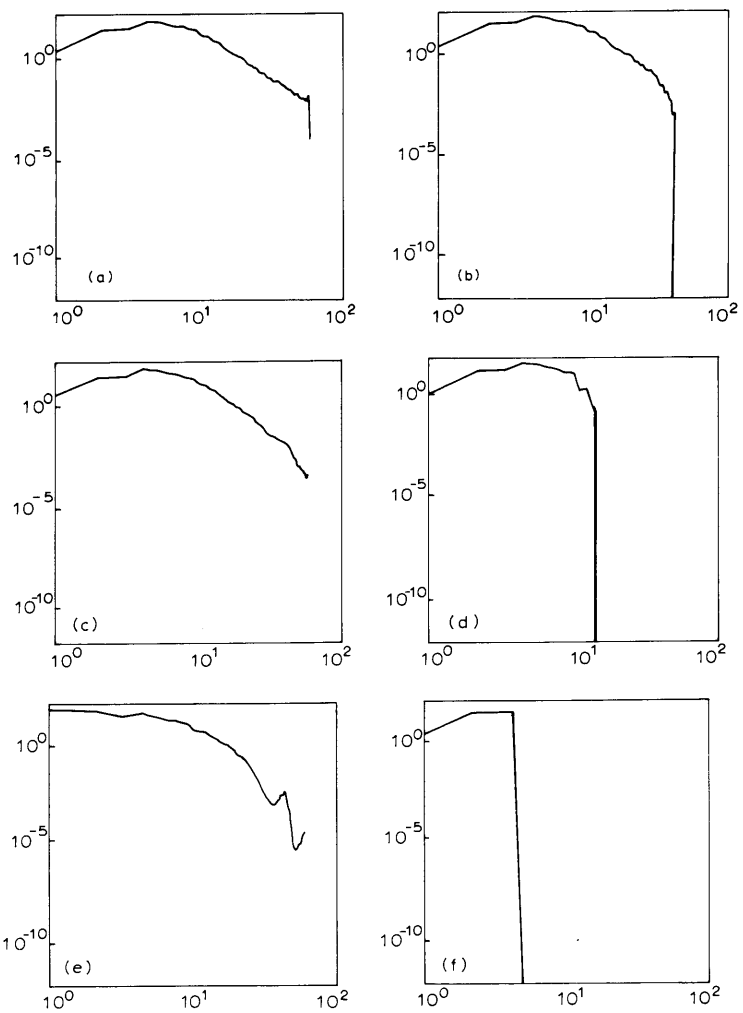

Fig. 4. Energy spectra: strong components at $t = 0$. (a) Wavelet packet: 50% strongest, (b) linear Fourier: lowest-wavenumber 50%, (c) wavelet packet: 5% strongest, (d) linear Fourier: lowest-wavenumber 5%, (e) wavelet packet: 0.5% strongest, (f) linear Fourier: lowest-wavenumber 0.5%.

presence of some dynamics. Much the same is true of the evolution of the theoretical dimension (figs. 13b, d, f), again indicating that significant interactions are taking place among the discarded components.

5.2. *Wavelet packet rank reduction*

5.2.1. *"Strong" components*

Next we turn to the results of experiments in which the basis chosen by the wavelet packet algorithm was employed for rank reduction. When the strongest 50% of the strong terms were retained (compression ratio 2), the resulting vorticity field evolution was very similar to the reference evolution. In particular, there is a single merged vortex at the center bottom of the final vorticity field (fig. 6a) just as in the reference (fig. 1b). The energy spectra are identical (compare fig. 1c and fig. 4a). The evolution from the rank-reduced field is both deterministically and statistically similar to that of the reference field (as seen by comparing the final

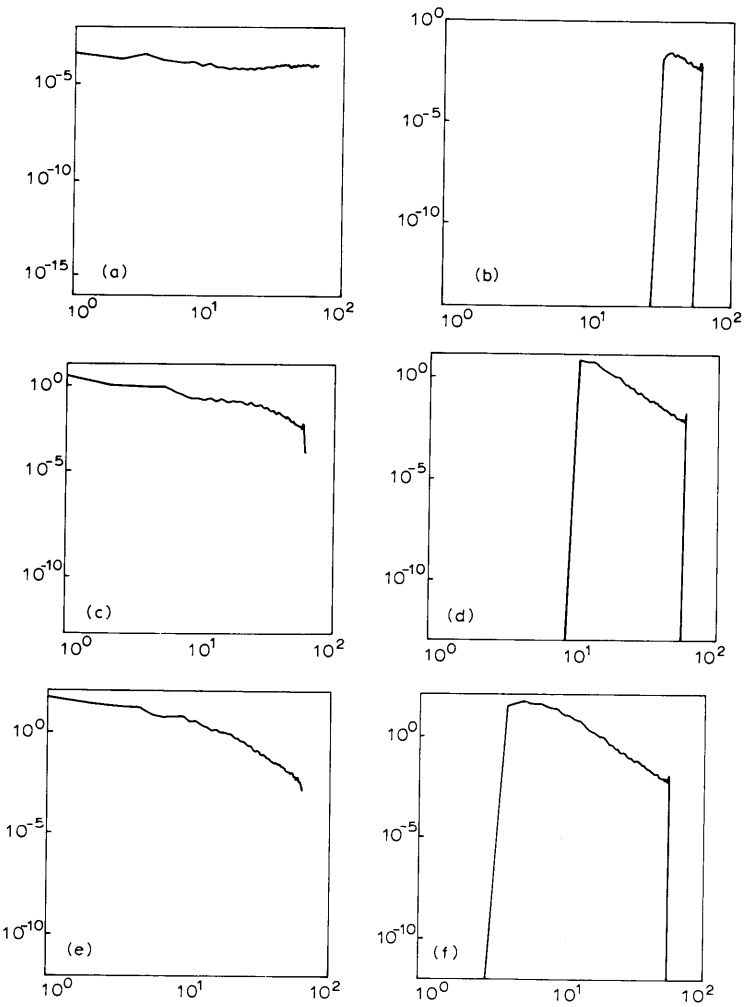

Fig. 5. Energy spectra: "weak" components at $t = 0$. (a) Wavelet packet: 50% weakest, (b) linear Fourier: highest-wavenumber 50%, (c) wavelet packet: 95% weakest, (d) linear Fourier: highest-wavenumber 95%, (e) wavelet packet: 99.5% weakest, (f) linear Fourier: highest-wavenumber 99.5%.

Fig. 6. Vorticity fields: "strong" components at $t = 0.6$. (a) Wavelet packet: 50% strongest, (b) linear Fourier: lowest-wavenumber 50%, (c) wavelet packet: 5% strongest, (d) linear Fourier: lowest-wavenumber 5%, (e) wavelet packet: 0.5% strongest, (f) linear Fourier: lowest-wavenumber 0.5%.

Fig. 7. Vorticity fields: "weak" components at $t = 0.6$. (a) wavelet packet: 50% weakest, (b) linear Fourier: highest-wavenumber 50%, (c) wavelet packet: 95% weakest, (d) linear Fourier: highest-wavenumber 95%, (e) wavelet packet: 99.5% weakest, (f) linear Fourier: highest-wavenumber 99.5%.

vorticity field in fig. 1b to that in fig. 6a, and comparing the spectra in fig. 1d to that in fig. 8a). Likewise, the enstrophy and theoretical dimension of both the rank-reduced and reference fields evolve in very similar ways (compare fig. 1e with fig. 10a, and fig. 1f with fig. 12a).

When the strongest 5% of the wavelet packet coefficients were retained (compression ratio 20), the results were statistically well-predicted, but deterministically poor. The rank-reduced initial field (fig. 2c) and its energy spectrum (fig. 4c) closely resemble the reference (fig. 1a and fig. 1c), but the final vorticity field exhibits significant differences (compare fig. 6c with fig. 1b) even though the energy spectra are very similar (compare fig. 8c with fig. 1d). We also observe that the enstrophy and theoretical dimension of the rank-reduced flow (fig. 10c and fig. 12c) are quite similar to the enstrophy and theoretical dimension of the reference (fig. 1e and fig. 1f).

When only the strongest 0.5% of the wavelet packets were retained (giving a compression ratio of 200), we found that the rank-reduced initial vorticity field differs markedly from the reference solution (compare fig. 1a with fig. 2e). After reduction, there remain only approxi-

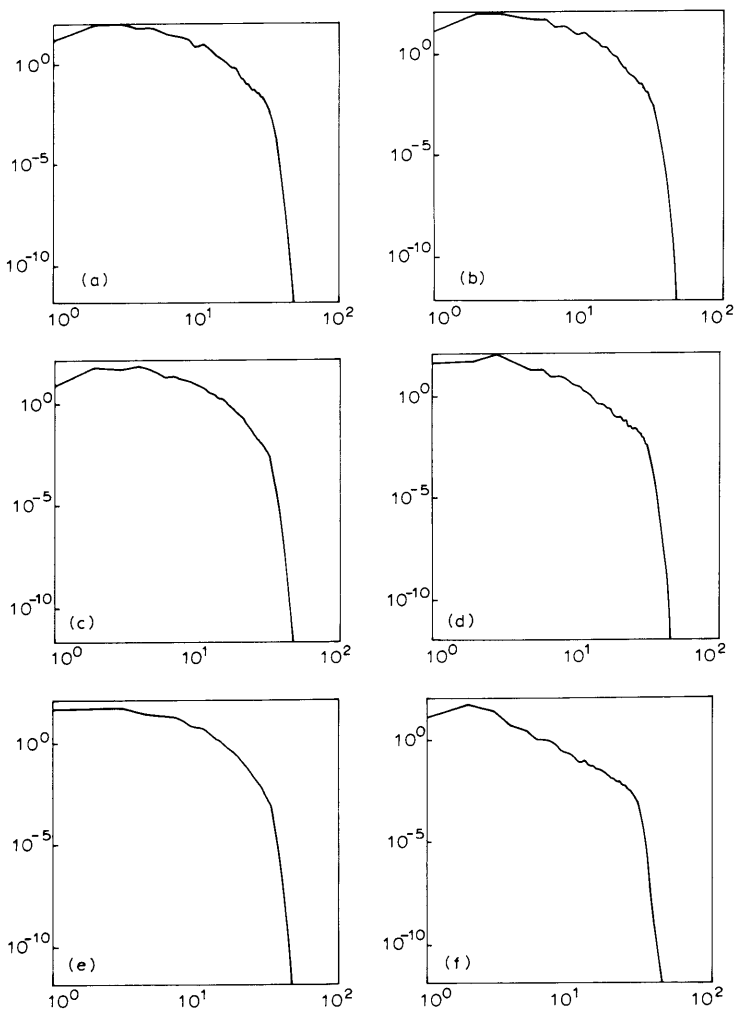

Fig. 8. Energy spectra: "strong" components at $t = 0.6$. (a) Wavelet packet: 50% strongest, (b) linear Fourier: lowest-wavenumber 50%, (c) wavelet packet: 5% strongest, (d) linear Fourier: lowest-wavenumber 5%, (e) wavelet packet: 0.5% strongest, (f) linear Fourier: lowest-wavenumber 0.5%.

mations to the coherent structures; in contrast to the linear Fourier reduction, the coherent structures retain their original regularity and are not eroded by smoothing. However, the vorticity filaments of the background have been removed. The rank-reduced vorticity field remains statistically similar to the reference in the sense that the spectrum remains the same (compare fig. 1c with fig. 4e). Furthermore, this statistical similarity is preserved by the evolution (compare the final energy spectra in fig. 1d and fig. 8e), even though the appearance of the final fields differ markedly (compare fig. 1b against fig. 6e). The enstrophy of the reduced initial field evolves in a manner similar to the reference (compare fig. 1e and fig. 10e). The theoretical dimension also behaves in a manner similar to the reference (fig. 1f and 12e), in the sense that both are slowly decreasing on average, with fluctuations which might be accounted for by vortex interactions. The theoretical dimension of the reduced flow field is much lower than that of the reference, because of the drastic reduction in the rank of the initial field.

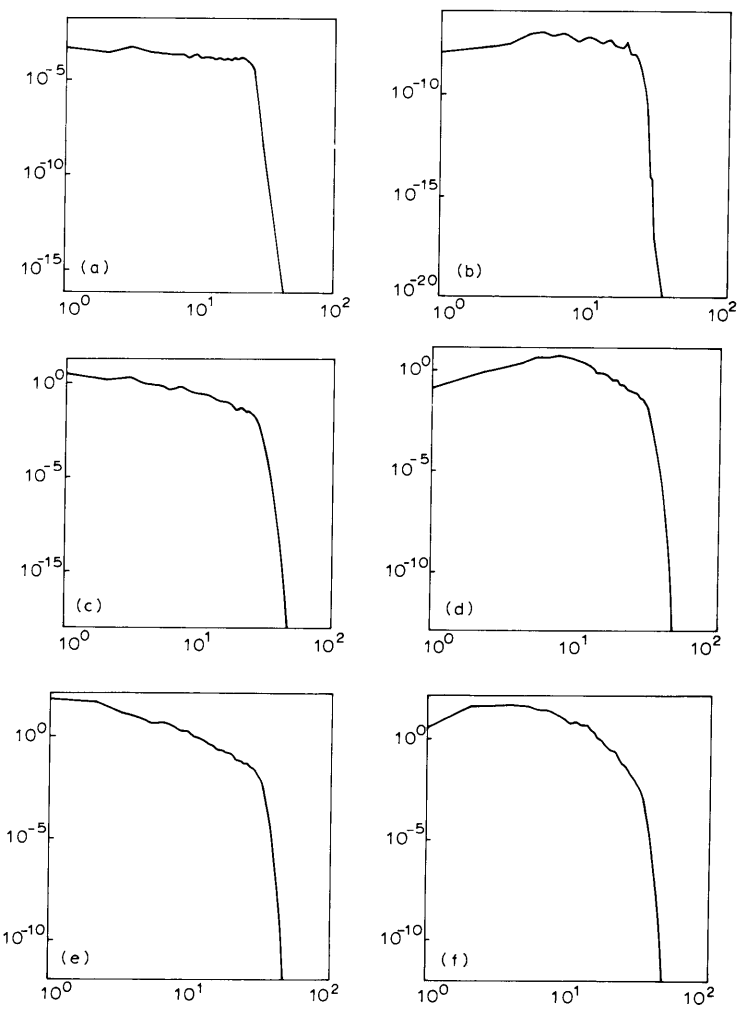

Fig. 9. Energy spectra: "weak" components at $t = 0.6$. (a) Wavelet packet: 50% weakest, (b) linear Fourier: highest-wavenumber 50%, (c) wavelet packet: 95% weakest, (d) linear Fourier: highest-wavenumber 95%, (e) wavelet packet: 99.5% weakest, (f) linear Fourier: highest-wavenumber 99.5%.

5.2.2. "Weak" components

Finally, we examine the evolution of the weakest wavelet packet components of the initial flow. If we retain the weakest 50% (fig. 3a) of the wavelet packets, the flow very rapidly dissipates the very smallest structures and after $t = 0.05$ remains frozen (see the final field in fig. 7a). The spectra at the start and at the end are nearly flat, and quite unlike the reference spectra (compare fig. 5a with fig. 1c, and fig. 9a with fig. 1d). Also, the enstrophy and theoretical dimension first decrease very rapidly and then behave almost like constants (figs. 11a and 13a), indicating an absence of strong interactions. If we retain the weakest 95% (fig. 3c) of the wavelet packets, the flow also dissipates rapidly up to $t = 0.05$, and then moves very slowly with feeble interactions (see the final field in fig. 7c). The spectra at the start and at the end are all quite different from that of the reference (compare fig. 5c with fig. 1c, and fig. 9c

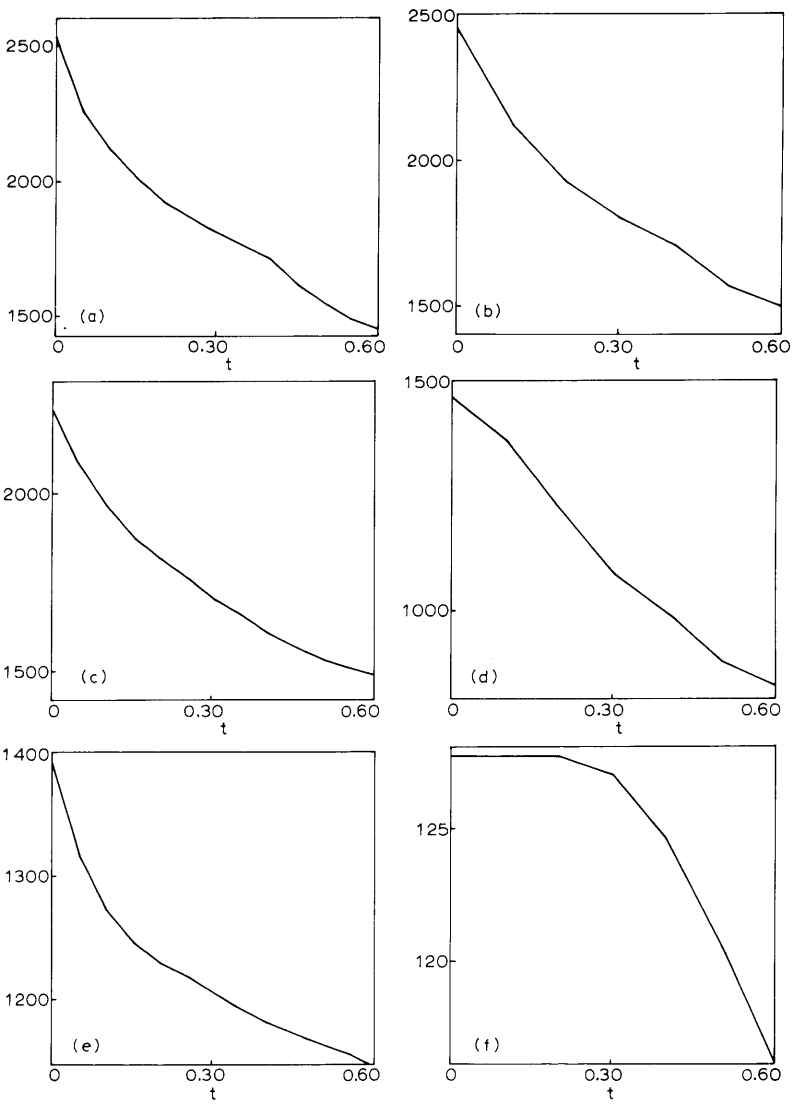

Fig. 10. Evolution of enstrophy: "strong" components. (a) Wavelet packet: 50% strongest, (b) linear Fourier: lowest-wavenumber 50%, (c) wavelet packet: 5% strongest, (d) linear Fourier: lowest-wavenumber 5%, (e) wavelet packet: 0.5% strongest, (f) linear Fourier: lowest-wavenumber 0.5%.

with fig. 1d), though the spectral slope about -1 in the inertial region suggests white noise. Again, the enstrophy and theoretical dimension behave much more like constants after a rapid initial decrease (figs. 11c and 13c), indicating an absence of strong interactions. In the third case (fig. 3e), in which the weakest 99.5% of the wavelet packets are retained, the flow is slowly varying and exhibits occasional merging. The initial (fig. 5e) and final spectra (fig. 9e), with spectral slope roughly -2 in the inertial region, bore some resemblance to those of the reference (fig. 1c and fig. 1d), where the spectral slope is roughly -4. The enstrophy and theoretical dimension also behave somewhat like the reference (compare fig. 11e with fig. 1e, and fig. 13e with fig. 1f), indicating that the components discarded by such a drastic, 200-fold, rank reduction do contribute somewhat to the dynamics.

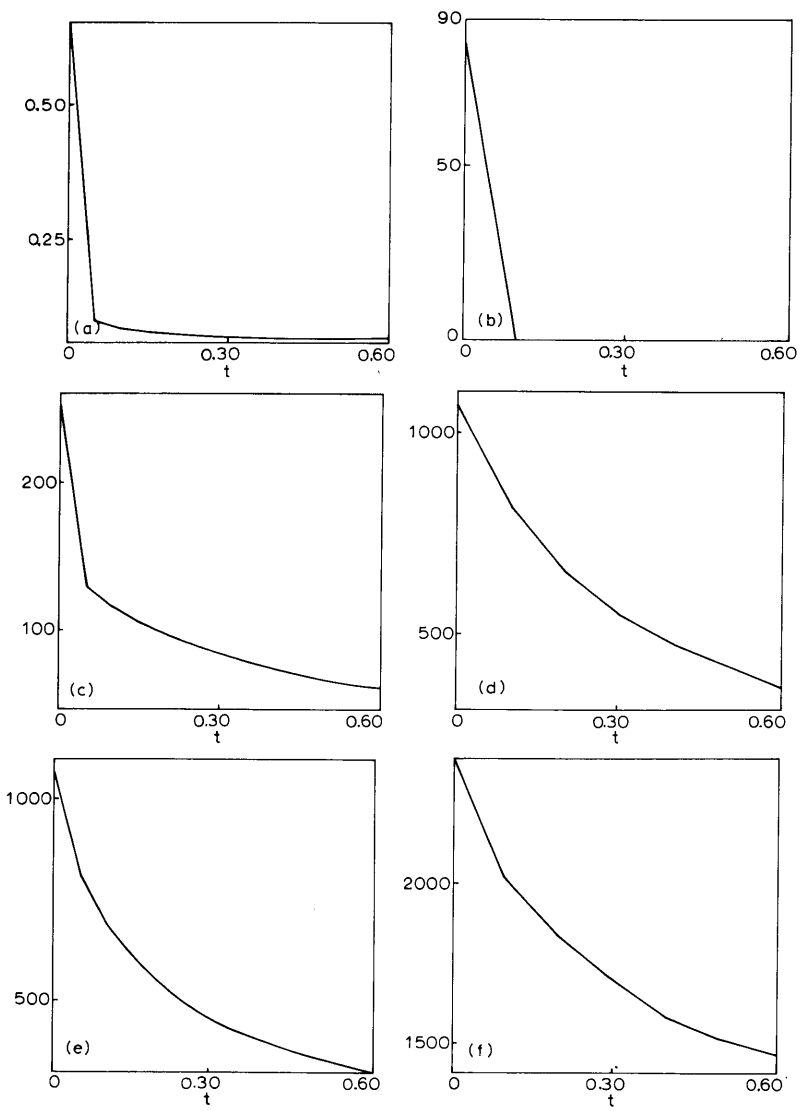

Fig. 11. Evolution of enstrophy: "weak" components. (a) wavelet packet: 50% weakest, (b) linear Fourier: highest-wavenumber 50%, (c) wavelet packet: 95% weakest, (d) linear Fourier: highest-wavenumber 95%, (e) wavelet packet: 99.5% weakest, (f) linear Fourier: highest-wavenumber 99.5%.

These results indicate that the wavelet packet algorithm is useful, not only for representing the instantaneous flow efficiently, but also for identifying the dynamically. important flow components. Those actually correspond to the coherent structures. Vorticity filaments can be neglected because they are only slaved modes, produced by interactions among the coherent structures and then passively advected by them. The connection between coherent structures present in the vorticity field and the nonlinearities of the Navier–Stokes dynamics becomes apparent when they are visualized together in physical space. In running a video movie of their evolution (cf. remark on data below), one observes bursts of nonlinearities when coherent structures strongly interact, such as same-sign vortex merging or opposite-sign vortex binding. This observation suggests that, to improve predictability of the low-rank models of two-dimensional turbulent flows, we should use bases which retain much of the local information, like precise amplitudes and positions, attached to the coherent structures. By contrast, the background flow of vorticity filaments may be neglected, or parametrized by an ad hoc statistical model.

6. Conclusion

In conclusion, the predictability of a turbulent flow using a post hoc reduced-rank approximation depends upon the choice of basis in which the rank reduction of the initial

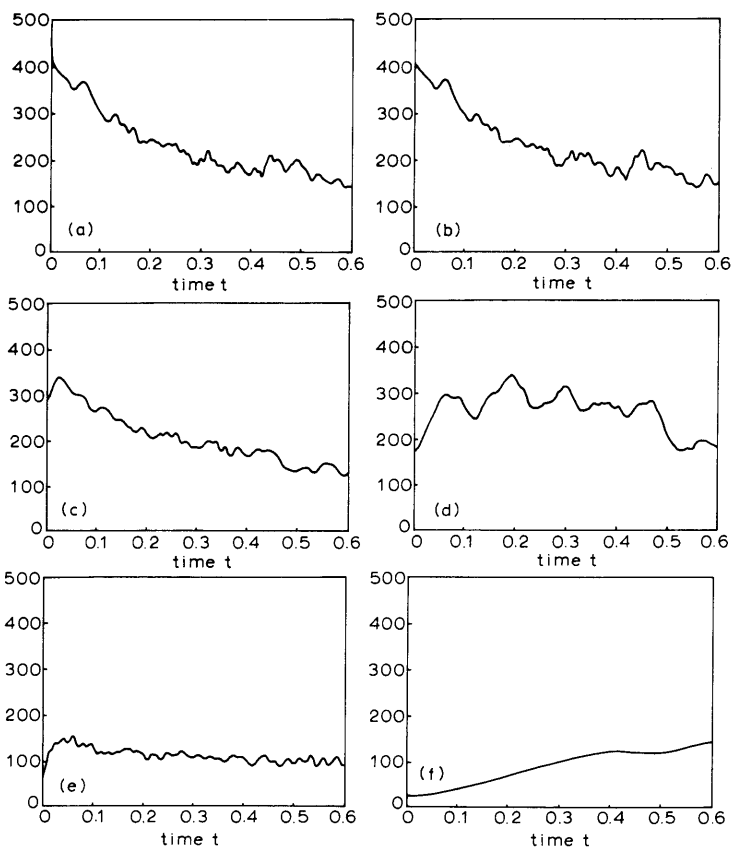

Fig. 12. Evolution of theoretical dimension: "strong" components. (a) Wavelet packet: 50% strongest, (b) linear Fourier: lowest-wavenumber 50%, (c) wavelet packet: 5% strongest, (d) linear Fourier: lowest-wavenumber 5%, (e) wavelet packet: 0.5% strongest, (f) linear Fourier: lowest-wavenumber 0.5%.

state is performed. In the case of two-dimensional turbulent flows, we have compared linear Fourier and top-few wavelet packet rank-reduction methods, and we have found wavelet packets to be superior for various kinds of approximation. We have illustrated that keeping the strongest best-basis wavelet packets retains the dynamically active features of coherent structures. Linear Fourier rank reduction, on the other hand, smooths the coherent structures and thereby removes dynamically vital features.

Using the best basis of wavelet packets, the reduction of the number of parameters necessary to describe the dynamics is done without assuming any scale separation. This contrasts with large-eddy simulation, or nonlinear slow manifold projection as used in weather forecasting [8], or approximate inertial manifolds [10,5]. All of these other methods presently assume Fourier scale separation in order to work, namely that high wavenumber modes are slaved by low wavenumber modes.

There are two directions to follow in the future. The first one, let us call it the *analytical* approach, is to examine a very large number of turbulent flows, both computed and measured, in order to identify and classify those molecules or coherent states which are most commonly encountered. The first approach has been explored with Karhunen–Loève methods in the work of Aubry et al. [1] and Sirovich and Sirovich [9]. Our methods are very similar in spirit, only computationally more efficient (O(N log N) versus N^3). The other, let us call

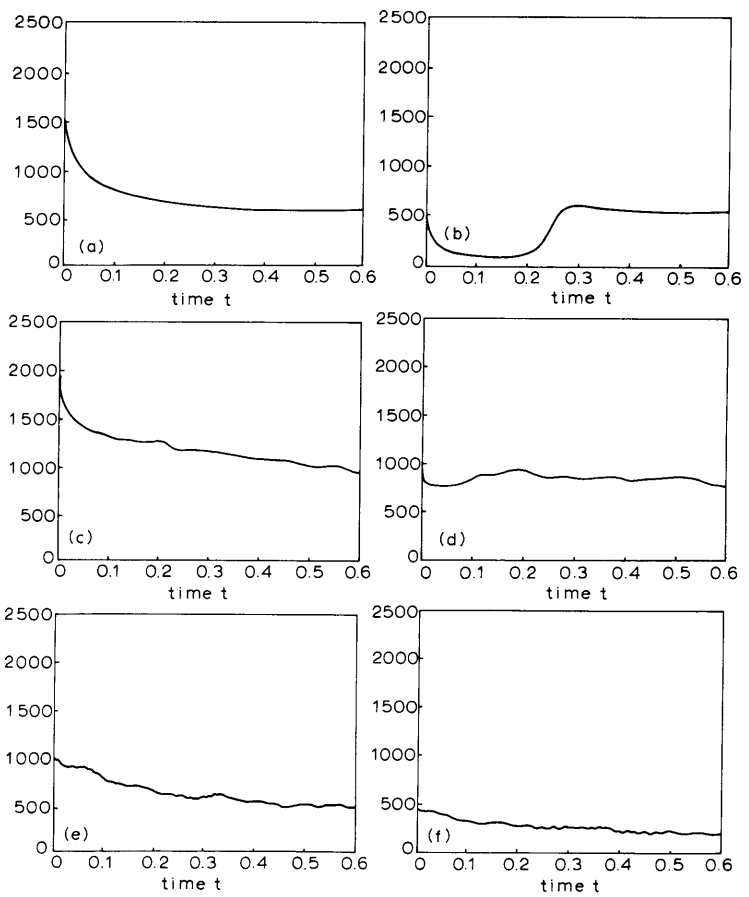

Fig. 13. Evolution of theoretical dimension: "weak" components. (a) Wavelet packet: 50% weakest, (b) linear Fourier: highest-wavenumber 50%, (c) wavelet packet: 95% weakest, (d) linear Fourier: highest wavenumber 95%, (e) wavelet packet: 99.5% weakest, (f) linear Fourier: highest-wavenumber 99.5%.

it the *synthetic* approach, is to compute the evolution of flows from arbitrary initial distributions of phase space atoms, and then observe what types of molecules get formed. We shall discuss the computation of flow field evolutions in terms of atomic parameters in a future paper.

Data. The visualizations of the evolving vorticity fields and their various rank reductions are available on VHS videotape, in PAL, SECAM, and NTSC formats, for US $25. To order, contact CNRS Audiovisuel, Dept. Diffusion, 1 Place Aristide Briand, 92195 Meudon Cedex, France, telephone (33)-1-45.07.56.86, fax (33)-1-45.07.59.00.

Acknowledgement

The numerical experiments were performed on the Cray 2 at the Centre de Calcul Vectoriel pour la Recherche, using the incompressible Navier–Stokes code of Claude Basdevant. The color visualizations were done in collaboration with Jean-François Colonna.

References

[1] N. Aubry, P. Holmes, J.L. Lumley and E. Stone, The dynamics of coherent structures in the wall region of a turbulent boundary layer, J. Fluid Mech. 192 (1988) 115–173.
[2] R.R. Coifman, Y. Meyer, and M.V. Wickerhauser, Wavelet analysis and signal processing, Wavelets and Their Applications, eds. Ruskai et al. (Jones and Bartlett, Boston, 1992).
[3] R.R. Coifman and M.V. Wickerhauser, Entropy based methods for best basis selection, IEEE Trans. Information Theory (March, 1992).
[4] I. Daubechies, Orthonormal bases of compactly supported wavelets, Commun. Pure Appl. Math. 41 (1988) 909–996.
[5] C. Foiaş, O. Manley and R. Temam, Attractors for the Bénard problem: existence and physical bounds on their fractal dimension, Nonlinear Anal. Theory. Methods Appl. 11 (1987) 939–967.
[6] S.G. Mallat, A theory for multiresolution signal decomposition: the wavelet decomposition, IEEE Trans. Pattern Anal. Machine Intelligence 11 (1989) 674–693.
[7] Y. Meyer, De la recherche pétrolière à la géometrie des espaces de Banach en passant par les paraproduits, preprint, École Polytechnique, Palaiseau, Seminaire équations aux dérivées partielles (1985–1986).
[8] B.A. Machenhauer, On the dynamics of gravity oscillations in a shallow water model with applications to normal mode initialization, Beitr. Phys. Atmos. 10 (1977) 253–271.
[9] L. Sirovich and C.H. Sirovich, Low dimensional description of complicated phenomena, Contemp. Math. 99 (1989) 277–305.
[10] R. Temam, Approximation by attractors, large eddy simulations and multiscale methods, Proc. R. Soc. A 434 (1991) 23–39.
[11] M.V. Wickerhauser, High-resolution still picture compression (Digital Signal Processing, 1992), to appear.